

Biomedical Convergence Facilitated by the Emergence of Technological and Informatic Capabilities

Dong Yang^{a,1}, Ioannis Pavlidis,² and Alexander Michael Petersen^{a,1}

¹*Department of Management of Complex Systems, Ernest and Julio Gallo Management Program,
School of Engineering, University of California, Merced, California 95343, USA*

²*Computational Physiology Laboratory, University of Houston, Houston, Texas 77204, USA*

We analyzed Medical Subject Headings (MeSH) from 21.6 million research articles indexed by PubMed to map this vast space of entities and their relations, providing insights into the origins and future of biomedical convergence. Detailed analysis of MeSH co-occurrence networks identifies three robust knowledge clusters: the vast universe of microscopic biological entities and structures; systems, disease and diagnostics; and emergent biological and social phenomena underlying the complex problems driving the health, behavioral and brain science frontiers. These domains integrated from the 1990s onward by way of technological and informatic capabilities that introduced highly controllable, scalable and permutable research processes and invaluable imaging techniques for illuminating fundamental structure-function-behavior questions. Article-level analysis confirms a positive relationship between team size and topical diversity, and shows convergence to be increasing in prominence but with recent saturation. Together, our results invite additional policy support for cross-disciplinary team assembly to harness transdisciplinary convergence.

The codification of knowledge facilitates more efficient search across the vast space of possible creative inputs accessible to scientists [1] – conceived in research as strategic configurations of established and new entities, relationships, tools, equipment, methods, processes, observation, theory, etc. Organization of knowledge into an ontology facilitates additional understanding of its structure, dynamics and future trajectories [2–4], as such knowledge maps [5–8] improve scientists’ ability to establish and recall complex relationships [9]. The pervasive drive to document entities and their relationships in detailed *-omics* atlases will thereby help scholars manage the increasing volume and pace of knowledge production [10, 11] and accelerate breakthrough discovery [12, 13] by helping scholars manage the uncertainty associated with exploration [14, 15].

Against this backdrop, we developed network-based methods for assessing the evolution of biomedical innovation. As the field of biology transitions from its descriptive roots into a health innovation frontier, research increasingly combines tacit inputs involving trial, error and practice (e.g. manual laboratory techniques) with explicit inputs that are highly transmissible and modifiable (e.g. pre-assembled computer algorithms). Consequently, the theory of recombinant innovation [1] provides a powerful framework for understanding the potency, and uncertainty, embodied by combinatorial approaches to search, refinement, experiment and discovery. Likewise, the triple-helix model of innovation [16–18] establishes the importance of catalysts for bringing potent opportunities – i.e., challenging problems demanding novel solutions met with a diverse supply of research approaches – to fruition. The catalysts in the present context are techno-informatic capabilities, characterized by highly controllable, scalable and permutable research processes for exploring and testing the exponentially vast number of biological interactions.

In order to prime the pump, national innovation systems have increased investment into transdisciplinary *convergence science* [19], a paradigm prescribed by its originators as “the coming together of insights and approaches from originally distinct fields” [20, 21] – as opposed to subfield integration characteristic of interdisciplinary approaches [22–24]. Stimulation of potent triple-helix configurations aims to support the emergence of new hybrid disciplines [25], for addressing complex global challenges [26]. Recombinant innovation is fundamental to the *convergence science* value proposition, as integrating diverse teams of experts hedges against uncertainty underlying the exploration process [27] and provides a testable mechanism [28, 29] for explaining the propensity of larger teams producing higher impact science [30]. By way of example, the advantage of cross-disciplinary integration was evident in full force during the genomics revolution, wherein traditional biologists and computer scientists leveraged familiar operational language to overcome relatively large epistemic and cultural distances between their traditionally distinct fields [28]. Recent work lends further support to cross-disciplinarity [27, 28] as the more impactful convergence mode for exploring across long disciplinary distances [29], as compared to expansive learning approaches [31] pursued by mono-disciplinary teams.

It is generally appreciated that techno-informatic capabilities will transform many research domains, in addition to biomedicine. Yet even in the case of the latter, we lack high-resolution maps for understanding the rich history and future potential of cross-domain integration. Hence, to identify and map the anatomy of biomedical convergence, we analyzed millions of intra-article keyword combinations using the high-resolution Medical Subject Heading (MeSH) classification system [32, 33], a controlled thesaurus maintained by the U.S. National Library of Medicine (NLM) and implemented within the ~30 million articles indexed by PubMed. By visualizing MeSH co-occurrence networks and measuring inter-article MeSH diversity over the last half century, we identified the dominant knowledge configurations underlying contemporary convergence. Notably, we document how Technology (captured by MeSH branch J) and Informatics (MeSH Branch L) emerged as convergence bridges, transforming non-invasive imaging, high-throughput anomaly detection, and big data integration – all key tools that are critical to addressing challenges at the frontiers of health, behavioral and brain science [29].

[a] These authors contributed equally; Send correspondence to: apetersen3@ucmerced.edu

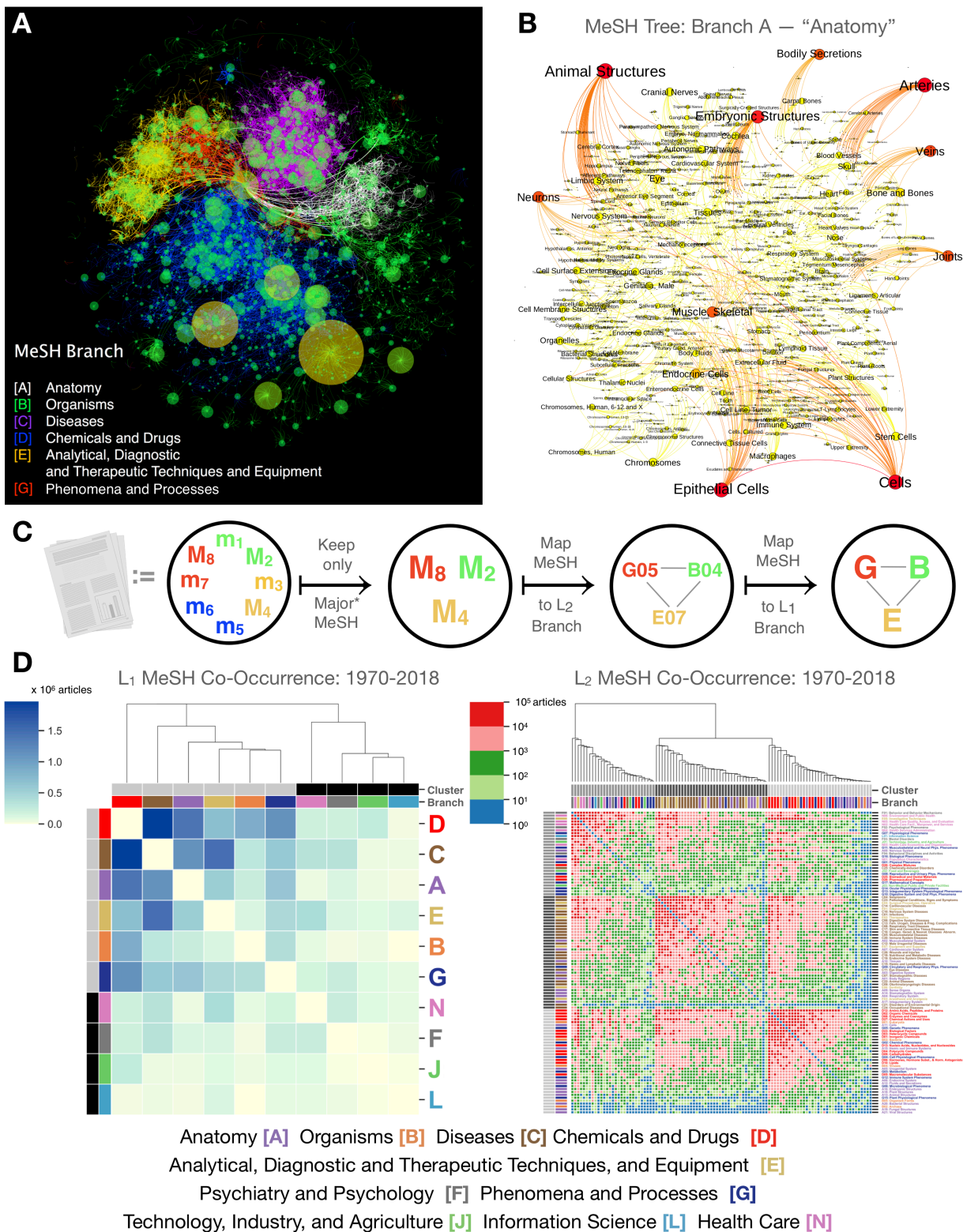


FIG. 1: Biomedical Knowledge Network. (A) Explicit network structure defined by the Medical Subject Heading (MeSH) tree implemented by the US National Library of Medicine across the PubMed index. Visualized is the quasi-hierarchical MeSH-MeSH network composed from the six traditional biomedical branches. (B) Network visualization of the “Anatomy” subtree (branch A). Nodes are individual MeSH and links are prescribed by the NLM MeSH Tree; nodes sized and shaded according to node degree. (C) Serial refinement of the MeSH appearing within each PubMed article: the set of MeSH \vec{m}_p for each article p are refined to just the Major “keywords” (indicated within PubMed by an asterisk *); these Major MeSH \vec{m}_p^* are readily mapped to their parent MeSH at the 2nd-level (L_2) and 1st-level (L_1). (D) Historical MeSH co-occurrence frequencies for articles and reviews at the L_1 and L_2 levels; MeSH branches indicated by color-scale border segments (note the different color schema than in panel A). MeSH clusters are determined by a modularity maximizing algorithm [34] and indicated by the gray-scale border segments; hierarchical structure indicates the minimum spanning tree representation of each co-occurrence matrix; entities are sorted within cluster in decreasing order of prevalence, calculated as the sum of co-occurrences with all other MeSH.

Quantitative Framework

Related ontology and diversity research. Prior scientific ontology studies use journal and article classification systems of varying granularity and specificity levels. A common objective is to measure disciplinary diversity by using classification systems as proxies for research topic subject areas, and measuring category-category correlations [35, 36]. Some studies utilize broadly defined categories, such as the journal-level “Subject Category” descriptors implemented within Web of Science [37–39], or article-level systems used within multi-disciplinary journals such PNAS [40] and PLOS ONE [41]. Another stream of research utilizes more high-resolution article-level classification systems, such as keywords [24], International Patent Classification (IPC) and US Patent Office Classification (USPC) codes [1, 42–44], MeSH [8, 18, 33, 40, 45, 46] and Physics and Astronomy Classification Scheme (PACS) codes [23]. Other approaches include topic mapping based on co-word analysis [47] and hybrid approaches integrating keywords and cited references to group research into knowledge clusters [7].

The MeSH tree. We operationalize the representation of the biomedical knowledge network using article-level MeSH annotations, which can be considered as keywords with varying specificity that are interrelated within a quasi-hierarchical tree illustrated in Fig. 1(A). The official MeSH tree is maintained by the NLM and consists of 16 branches designated by the characters A, B, C, D, E, F, G, H, I, J, K, L, M, N, V, Z (see <https://meshb.nlm.nih.gov/treeView> to explore the tree). The six branches A, B, C, D, E, G represent core biological entities, concepts and methods; whereas the branches F, J, L, N represent peripheral domains comprised also of entities, concepts and methods.

Previous studies focused on MeSH belonging to specific branch subsets, such as C, D and E [18, 33]. Here we exclude MeSH from the H, I, K, M, V, Z branches, as these are comprised of non-technical MeSH such as H (“Disciplines and Occupations”) and V (“Publication Characteristics”) – see Fig. S1 for a schematic representation of the quasi-hierarchical MeSH tree. To illustrate branch substructure, Fig. 1(B) shows the explicit MeSH-MeSH relations endowed in the MeSH tree for branch A (“Anatomy”). This particular branch is dominated by biophysical structures and their attributes – i.e., representing one half of the structure-function dichotomy, with branch G (“Phenomena and Processes”) representing the other half.

Article-level Data. Our comprehensive analysis is based upon the 2020 PubMed index consisting of more than 30 million index entries, with 93% of these classified as “Journal Article” or “Review”. We then pruned this dataset of articles lacking Major MeSH and focused on the sample spanning 1970-2018, resulting in 21.6 million publications (for additional details see *Methods*). Regarding notation, in what follows we use subscript p to indicate article-level information such as publication year, indicated by y_p ; the number of coauthors, k_p ; and the set of MeSH “keywords”, represented as a vector \vec{m}_p with 29,638 elements, each representing a distinct MeSH term. An article with the sample average of 4 Major MeSH terms corresponds to $\sum_i \vec{m}_{p,i} = 4$.

Projecting MeSH onto 10 Subject Areas (SA). We analyzed all MeSH belonging to the 10 core and peripheral branches. We refer to these broad knowledge domains as *Subject Areas* (SA). These SA represent a basis set for classifying MeSH according to their first-level parent branches (denoted by L_1). The MeSH tree is quasi-hierarchical (containing a relatively small number of loops), with 12 hierarchical levels per branch [33]. Hence, based upon this explicit relational tree structure, we can map any MeSH occurring at the third level or greater to its corresponding second-level (L_2) MeSH term, for which there are 104 types.

Figure 1(C) illustrates the full process for producing $\vec{S}A_p$, which begins with first pruning out minor MeSH terms and auxiliary qualifiers, leaving just Major MeSH terms that represent the article’s core SA decomposition. By way of example, the MeSH term “Obesity” has four Tree Number locators corresponding to three SA (C, E and G): C18.654.726.500; C23.888.144.699.500; E01.370.600.115.100.160.120.699.500; G07.100.100.160.120.699.500 (see Fig. S1). Hence, the L_2 representation of this single MeSH term is then given by {C18, C23, E01, G07} (which are each distinct MeSH terms among the 29,638). We catalogue these MeSH using a L_2 count vector, denoted by $\vec{S}A_p^{(2)}$, which contains 104 elements. Further projecting this set to its L_1 representation yields {C, C, E, G}, represented by $\vec{S}A_p^{(1)} = \{0,0,2,0,1,0,1,0,0,0\}$. This example highlights the nuanced organizational structure of the MeSH tree, where terms can span multiple SA and contexts, thereby giving rise to relatively small yet non-trivial cross-branch connectivity within the explicit MeSH knowledge network – see Fig. S2 for a network visualization of the explicit MeSH-MeSH relations within core biological SA. Combining multiple MeSH into $\vec{S}A_p$ yields a quantitative signature of each article’s SA composition.

Results

MeSH Co-Occurrence at the L_1 and L_2 levels. We assessed the entire space of MeSH combinations by tallying SA co-occurrences among the present (non-zero) elements contained in $\vec{S}A_p^{(1)}$ and $\vec{S}A_p^{(2)}$. Continuing with the example above, consider the SA counts {C, C, E, G}, which could arise from an article with a single Major MeSH annotation of “Obesity”, or an article with four Major MeSH mapping individually to the same set of SA; we do not distinguish between these two cases. We then tabulate the SA co-occurrences by counting for all unique SA-SA dyad types. In such a case, we tabulate three co-occurrence types: CE, CG and EG. When aggregating co-occurrence tallies across articles, we combine normalized tallies – e.g. by assigning

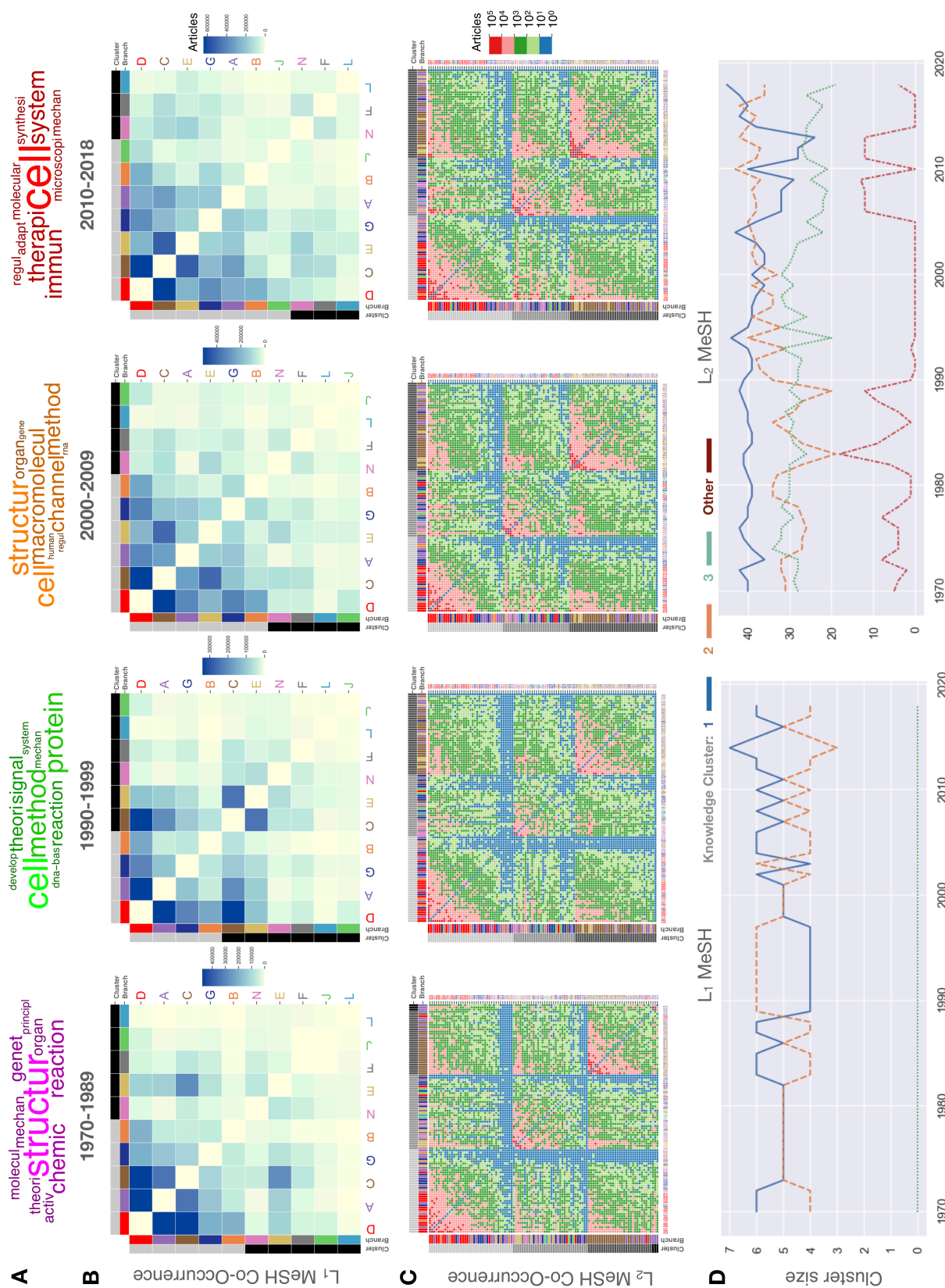


FIG. 2: Structure and Dynamics of MeSH-MeSH Co-occurrence. (A) Top 10 most frequent destemmed keywords from Chemistry and Physiology or Medicine Nobel Prize rational statements, sized proportional to their prevalence, illustrating the transition from structural to mechanistic orientation of grand scientific pursuits. (B,C) MeSH branches are indicated by axis labels with corresponding color-scale border segments; MeSH clusters determined by the Louvain modularity maximizing algorithm [34] are indicated by the outer gray-scale border segments. MeSH are ordered within cluster in decreasing order of prominence corresponding to total number of article instances for a given period, as indicated by the numerical scales. (B) L_1 co-occurrence matrices show sequential dynamics across 4 non-overlapping periods; linear color-scale. (C) L_2 co-occurrence; logarithmic color-scale. (D) Co-occurrence cluster size dynamics by year and resolution level: L_1 (left) and L_2 (right).

Anatomy [A] Organisms [B] Diseases [C] Chemicals and Drugs [D] Analytical, Diagnostic and Therapeutic Techniques, and Equipment [E] Psychiatry and Psychology [F] Phenomena and Processes [G] Technology, Industry, and Agriculture [J] Information Science [L] Health Care [N]

1/3 weight to the CE, CG and EG matrix elements in the example above – so that each article contributes a total weight of 1 to the co-occurrence matrix $M^{(1)}$ (and similarly for $M^{(2)}$ constructed at L_2). In this way, the total sum across matrix elements of M is proportional to the total number of articles analyzed in the sample; see the *Methods* section *Major MeSH Descriptors* for further details.

To begin, **Fig. 1(D)** shows co-occurrence frequencies recorded in the symmetric matrices $M_{1970-2018}^{(1)}$ and $M_{1970-2018}^{(2)}$, calculated across articles published between 1970-2018. Each matrix indicates the SA name along the right border, accompanied by a consistent color indicating the corresponding L_1 branch, useful for guiding visual inspection. We grouped SA into knowledge clusters using the Louvain modularity maximizing algorithm [34], indicated by the gray-scale border segments along the upper and left matrix borders. The top border contains hierarchical clustering trees indicating the minimum spanning tree representation of each matrix. To further aid visual inspection, we maintain the gray-scale cluster shades across the aggregate matrices shown in **Figs. 1** as well as the time-disaggregated matrices visualized in **Fig. 2**.

As such, we analyzed MeSH co-occurrences at both the L_1 and L_2 levels, thereby producing knowledge network maps with complementary degrees of granularity. The main result for L_1 is the two-SA substructure observed for $M_{1970-2018}^{(1)}$. This substructure confirms that D, C, A, E, B and G form a core biomedical cluster, with the peripheral application domains N, F, J and L forming a second cluster.

At higher resolution, the L_2 matrix $M_{1970-2018}^{(2)}$ features three mixed clusters. The first cluster is comprised of a wide array of L_2 MeSH pertaining to complex human phenomena related to behavior, physiology and health. Importantly, this cluster also includes L01 (“Information Science”) and J01 (“Technology, Industry, and Agriculture”). Because these are two focal domains in our analysis, we refer to their MeSH scope notes to provide additional context. According to MeSH scope notes, “Technology” refers to “the science and application of techniques” (J01), and more specifically “the application of scientific knowledge to practical purposes in any field [including] methods, techniques, and instrumentation” (J01.897). Likewise, MeSH scope notes describe “Information Science” (L01) as “The field of knowledge, theory, and technology dealing with the collection of facts and figures, and the processes and methods involved in their manipulation, storage, dissemination, publication, and retrieval.”

The second cluster is comprised of diagnostic methods associated with particular diseases and the systems they affect, as represented by MeSH primarily from branches A (“Anatomy”), C (“Chemicals and Drugs”) and E (“Analytical, Diagnostic and Therapeutic Techniques, and Equipment”). The third cluster is comprised of biological entities and the phenomena that relate them, from cells to chemicals and the multi-scale processes that connect inputs, outputs and characteristics of their reaction environments.

Historical co-occurrence trends. The last half-century of biomedical research has witnessed incredible transition from a descriptive field – focused around identifying molecules, higher-order structures, reaction pathways and mediators – into a field seeking to identify holistic mechanisms underlying systemic abnormalities in an effort to develop pointed therapies. This transition is illustrated through the Nobel Prizes awarded for **Chemistry** and **Physiology or Medicine**, which up until the 1970s and 1980s predominantly awarded research documenting key structural entities and reactions. Based upon this early work, subsequent Nobel research has transitioned to addressing challenges at the nexus of the medical innovation triple helix – where societal demand and industrial supply for acute solutions are facilitated by technological capabilities [18].

To illustrate this point, **Fig. 2(A)** shows the top ten stemmed keywords from Nobel Prize “rationale” statements, identifying prominent contextual themes across the last half century. Indeed the 1980s brought forth novel imaging, laboratory control and synthesis technologies, fundamental in the 1990s to map the genetic blueprints encoding biological structure [28]. Polymerase chain reaction (PCR), among other high-throughput techniques, accelerated science to the realm of highly controllable, scalable and permutable processes that hitherto have been primarily restricted to traditional computational domains. Since then, the last twenty years has been marked by the rapid development of bioengineering capabilities, such as CRISPR gene editing tools [48] and powerful demonstration of stem cell pluripotency [49], which allow scientists to more precisely understand emergent structure-function relations, opening the door for synthetic biology applications [50] that (re)design biological systems [51] or even develop altogether new building blocks [52].

To visualize this history unfold, we disaggregated the MeSH co-occurrence data into four non-overlapping periods: 1970-1989, 1990-1999, 2000-2009 and 2010-2018. For each period we tabulate the co-occurrence matrix, denoted by $M_y^{(1)}$ ($M_y^{(2)}$), where y denotes a given period. **Figure 2(B)** illustrates the structural dynamics at the L_1 level, identifying branch E and J as vacillating domains switching between the two dominant clusters. The first L_1 cluster is characterized by D, A, G and B – largely descriptive SA, with the exception of “Phenomena and Processes” (G). The second cluster is comprised of N, F and L – peripheral SA which are increasingly convergent with the traditional SA, as indicated by extreme off-diagonal elements representing cross-domain integration.

At higher resolution, **Fig. 2(C)** shows the structural evolution of $M_y^{(2)}$, which is characterized by two relatively stable clusters and a more diverse and vacillating intermediate cluster. Note that MeSH are sorted within each cluster in decreasing order of prevalence, calculated as the sum of co-occurrence values across a given row of $M_y^{(2)}$. Notably, “Information Science” (L01) and “Technology, Industry, and Agriculture” (J01) are located in this intermediate cluster during the 1970-1989 period, where they play less dominant roles as indicated by their ranks within the cluster. However, over time their prominence within this

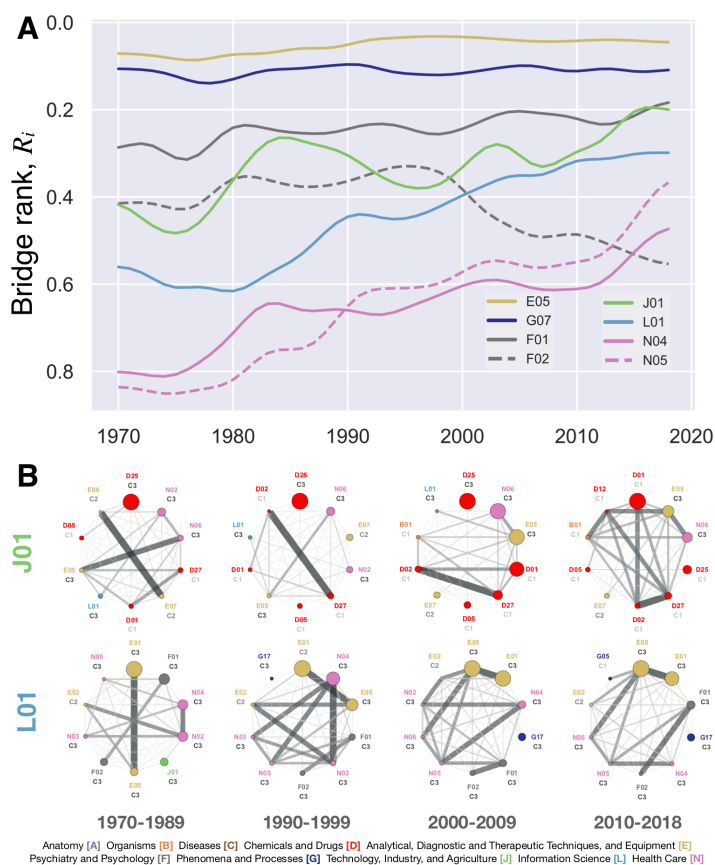


FIG. 3: Prominent convergence bridges. (A) For each MeSH, we analyzed the time series of bridge rank, $R_{i,t}$, a normalized ranking based upon the knowledge bridge score (β_i) defined in Eq. (1). Smaller rank values ($R_{i,t}$) correspond to larger β_i values, representing MeSH that are highly co-occurrent with MeSH belonging to other knowledge clusters. Plotted are smoothed time series to facilitate visual inspection. Notably, J01 and L01 are rapidly emerging convergence bridges arising from the highly generalizable, scalable and codifiable nature of techno-informatic tools and algorithms facilitating novel non-invasive imaging, high-throughput analysis, measurement, and data integration. Other MeSH shown here identify the emerging convergence nexus of Health Care (N04, N05) and Behavior (F01). (B) MeSH neighborhood subnetworks for J01 and L01 each show the ten most frequently co-occurring MeSH for the indicated period – sorted clockwise, starting from the top, with nodes sized proportional to $M_{ij}^{(2)}$; each MeSH’s SA is indicated by its node/label color. Links are plotted with thickness and shade proportional to $M_{ij}^{(2)}$, thereby indicating the cross-domain linkages among prominent neighbors that are facilitated by i . Each node includes its MeSH identifier and a knowledge cluster identifier, the latter indicated by a gray scale gradient. For example, MeSH J01 “Technology, Industry, and Agriculture” (which is a member of C3 for the first three periods and subsequently transitioning to C1 in the most recent period) is highly connected to MeSH from all other clusters (C1–C3), in particular to L01 until its disassociation in the most recent period 2010–2018; interestingly, L01 “Information Science” diverged from J01 as early as the first period 1970–1989, subsequently becoming more strongly coupled with members of branch E and G. See **Figs. S3–S4** for extended analysis of bridge ranks and neighborhood subnetworks for the remaining convergence bridges

cluster increases; by 2010–2018, J01 joined the biological agents and reactions cluster, characterized by the core “Amino Acids, Peptides, and Proteins” (D12), “Chemical Actions and Uses” (D27), “Eukaryota” (B01) and “Organic Chemicals” (D02). Close inspection reveals J01 having relatively strong co-occurrence with “Inorganic Chemicals” (D01), “Investigative Techniques” (E05), “Health Care Quality, Access, and Evaluation” (N06) and “Biomedical and Dental Materials” (D25) – indicative of a highly convergent applications nexus facilitated by technological capabilities.

Close inspection further reveals a similar transformation for L01, which rose to prominence from the 1980s onward, as genomics and other panoramic *omics* revolutions increased the demand for informatic solutions to map, characterize and associate entities into a functional atlas. This role did not merely manifest from increased technological capabilities associated with “Diagnosis” (E01) and “Investigative Techniques” (E05), but also involved the integration of powerful “Mathematical Concepts” (G17), in particular “Algorithms” (G17.035) to optimize classification and AI methods for “Deep Learning” (G17.485.500). Such methods are critical for capitalizing on new data-driven opportunities in Health Care (represented broadly by N04, N05, N06) for understanding “Behavior and Behavior Mechanisms” (F01).

Biomedical convergence identified by the emergence of cross-cluster bridges. To identify MeSH serving as bridges that link different knowledge clusters, we developed a metric which quantifies the degree to which individual nodes connect distinct clusters in a connected weighted network. This metric is motivated by the bridge centrality index [53]. We develop this approach with $M_t^{(2)}$ in mind, which is a complete network as opposed to a sparse network (See *Methods* section *Calculation of the cross-cluster bridge score* for further details). Applying this method to $M_t^{(2)}$ yields a knowledge bridge score for each MeSH and year, denoted by $\beta_{i,t}$, which is large if a MeSH is highly connected to clusters other than its own.

Figure 3 shows the rank dynamics $R_{i,t}$ (where larger $\beta_{i,t}$ correspond to smaller rank R_i) for 8 MeSH that are distinguished by either persistent growth or sustained prominence as knowledge bridges over the entire study period. Notably, L01 features steady growth following its emergence in the early 1980s, whereas J01 features an oscillating upward trend. We also observe a divergence between “Behavior and Behavior Mechanisms” (F01) and “Psychological Phenomena” (F02), with the latter becoming increasingly insular over the last 20 years. The emergence of health care bridges relating to “Health Services Administration” (N04), “Health Care Quality, Access, and Evaluation” (N05) and situational behavior analysis (F01) is another disruptive trend from the last decade – consistent with the ramp-up of several international *Human Brain Projects* [54, 55] in 2013, thereby championing the brain research nexus as the next frontier [29].

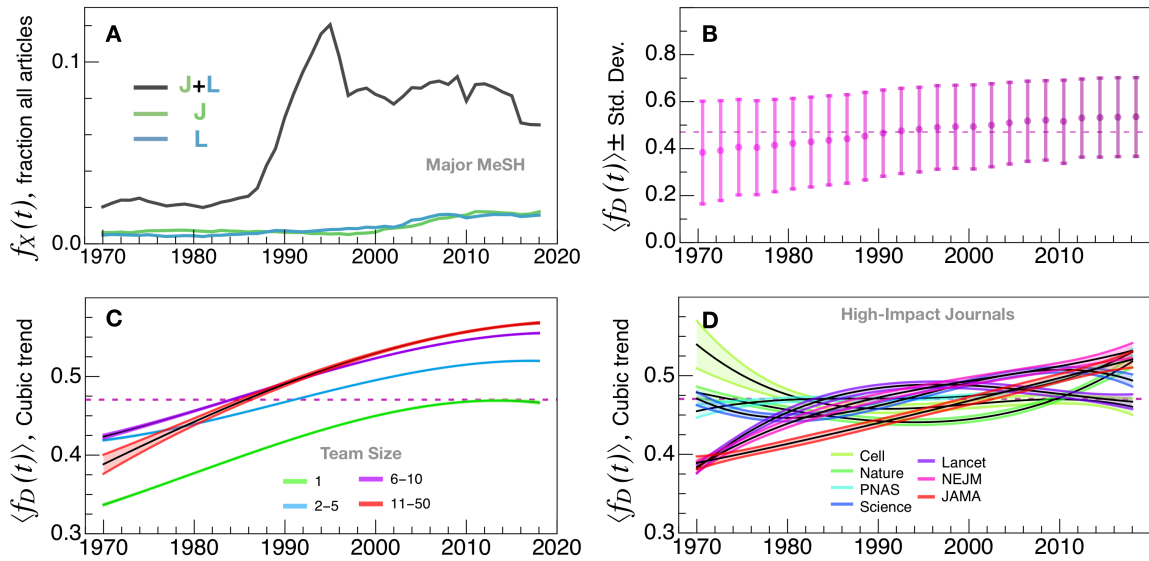


FIG. 4: Increasing prevalence of cross-domain knowledge integration. (A) Fraction of articles, $f_X(t)$, featuring at least half of Major MeSH in ABCDEG and at least a quarter in J, L or J+L. (B) $f_{D,p}$ measures article-level SA diversity, based on weighted pairwise SA-SA combinations defined in Eq. (S2). Average $f_{D,p}$ diversity value and standard deviation (error bar) calculated for non-overlapping 3-year windows over the period 1970–2018; the global average diversity value (0.47) is indicated by the horizontal dashed line. The mean value $\langle f_D(t) \rangle$ has increased from 0.38 to 0.53, representing 39.5% growth, over the entire 49-year sample period. (C) Increased knowledge diversity correlates with the emergence of team science, where the most rapid increase is among the larger teams with 11-50 coauthors. Solo-author research has only recently reached the average diversity value indicated by the horizontal dashed line. (D) Heterogeneous trends by longstanding core (Cell), elite multi-disciplinary (Nature, PNAS, Science) and biomedical (Lancet, NEJM, JAMA) journals. NEJM and JAMA show the largest consistent increase over time; Nature and PNAS exhibit the largest increase in the last decade. Each curve represents the third-order polynomial trend, with shaded colored areas indicating the 99% CI for each trend line.

Convergence factors – SA composition, prevalence, team size and scientific impact. The value proposition envisioned by convergence science originators [20] was novel configurations of experts strategically assembled to address a dimension of the underlying problem that would be otherwise inaccessible by mono-disciplinary strategies. The convergent union between biology and computing experts in the genomics revolution provides a rich example [28]. Hence, it follows that convergent research strategies are more likely to prevail in team science endeavors, and provides a testable mechanism for the propensity for larger teams to produce higher-impact science [30].

Indeed, the importance of informatic (L) and technological (J) capabilities to modern biomedical research cannot be understated. To illustrate the emergence of these bio-technological and bio-informatic modes, indicated by X , we calculated the fraction of articles by year that contain a significant component belonging to SA J and/or L. To ensure that the articles are otherwise focused on traditional biomedical SA, we estimate the number of cross-domain articles by focusing on the subset of PubMed articles featuring a half or more of their MeSH in the core categories ABCDEG. We then assign the indicator X to those articles which also contain at least a quarter of their MeSH belonging to L, J, or L+J in combination, and report the quantity of articles featuring X as the fraction $f_X(t)$ of the total articles by year.

Figure 4(A) indicates a burst of activity around the early 1990s for research containing both L and J in combination – much greater than the $f_X(t)$ calculated for either SA alone. This particular configuration of $ABCDEG \times J \times L$ represents a formidable nexus featuring the combination of high-throughput equipment to produce and churn through massive biomedical data. For comparison, **Fig. S5(A)** applies the same method to all MeSH (i.e., not distinguishing between Major and Minor MeSH), thereby including the more peripheral MeSH capturing the idiosyncratic research details. This second perspective indicates a more steady integration over time of J and L capabilities at the SA periphery, with the strongest upturn in J+L in the early 2000s, which has since saturated. Hence, if the 1990s brought forth the revolution in biomedical research, and the 2000s witnessed the further penetration of this paradigm shift, there appears to be a recent stagnation owing primarily to L which has permeated other convergence zones [56], such as computational social science [57] and the science of science [58].

To further explore the evolution of cross-domain SA configurations at the article level, we developed a Blau-like diversity measure, denoted by $f_{D,p}$, and based upon SA-SA co-occurrence. This measure accounts for two distinct diversity types – both categorical variation and concentration disparity [59]. Our method takes as input the categorical count vector \vec{S}_{A_p} and applies the outer tensor product, $\vec{S}_{A_p} \otimes \vec{S}_{A_p}$, yielding a weighted matrix \mathbf{D}_p that captures dyadic SA-SA co-occurrence; see *SI*

Appendix Eqs. (S1)-(S2) for further elaboration. To summarize, if an article’s MeSH descriptors are contained in just a single SA, then there will be only one single non-zero value contained in \mathbf{D}_p , which will occur along the matrix diagonal. Conversely, if the article features several SA, then off-diagonal elements represent cross-domain combinations. Hence, $f_{D,p}$ measures the relative fraction of off-diagonal to diagonal elements – with $f_{D,p} = 0$ corresponding to minimal diversity. Because more evenly distributed SA counts will yield relatively larger off-diagonal values, and hence larger $f_{D,p}$ value, it is both a measure of variation and disparity [59]. Moreover, $f_{D,p} \in [0, 1)$ is a bounded statistic with clear interpretation of the lower and upper bounds.

We computed $f_{D,p}$ based upon $\vec{S}A_p^{(2)}$ counts tallied for each publications in our PubMed sample (i.e. using the L_2 MeSH representation of an article). **Figure 4(B)** shows the evolution of the mean diversity value $\langle f_D(t) \rangle$ calculated for articles grouped by publication year, and shows a steady increase in SA diversity over the last half century. Analysis of the entire distribution of values, $P(f_{D,p,t})$, also exhibits a systematic positive shift across the range of $f_{D,p}$ values, and so the increase in the mean value is not just the result of an upper tail effect in the aggregate distribution. Rather, we observe a marked decrease in the prevalence of mono-SA articles characterized by $f_{D,p} = 0$ in the lower distribution tail – see **Fig. S5(B)**. This result is analog to the reduced frequency of single-authored research observed over the same period [30], indicative of the intense burden to integrate distant knowledge domains, a challenge that contributes to the disappearance of the “renaissance” solo genius [60, 61].

To assess how team size mediates article-level SA diversity, we disaggregated the data into four team-size groups: solo-author (coauthor number $a_p = 1$); small-sized team ($1 < a_p \leq 5$); medium team ($5 < a_p \leq 10$); and large team ($10 < a_p \leq 50$). **Figure 4(C)** shows the dominant trends in average diversity time series $\langle f_D(t) \rangle$ for each team size group, from 1970 to present. To facilitate visual comparison of the dominant trends, shown are each time series fit using a third-order polynomial: $\langle f_D(t) \rangle \equiv a + b(t - 1990) + c(t - 1990)^2 + d(t - 1990)^3$. Notably, the curve for solo-author team shows a significant systematic shift towards lower SA diversity values. From the mid-1980s onward, the curves are ordered according to team size group, with the largest teams achieving SA diversity levels far in excess of the unconditional average for the entire period, $\langle f_D \rangle = 0.47$ (indicated by the horizontal dashed line in each figure sub-panel). As a robustness check, **Fig. S5(C)** shows the journal-level relation between article-level SA diversity and mean journal team size for the 60 biomedical journals appearing in the set of top-100 journals ranked by 2018 Clarivate Analytics JCR Impact Factor, indicating a higher range of SA diversity associated with larger teams.

The wide variation in journal-level $\langle f_D \rangle_j$ indicates that support for convergence science is a feature of the distinct communities of expertise. While it is beyond the present study, we speculate that the multidisciplinary composition of a journal’s editorial board is likely to be a strong factor underlying the prevalence of convergence science featured in a particular journal. Among the most prestigious journals shown in **Fig. 4(D)**, several feature recent decline in $\langle f_D(t) \rangle$ over the last two decades, including Cell and the Lancet; contrariwise, the medical journals NEJM and JAMA are consistently trending upwards. To further illustrate the dynamics at the journal level, **Fig. S5(D)** shows the top-10 journals in terms of their largest growth in $\langle f_D(t) \rangle$ over the study period, featuring prominent journals in multiple domain areas including cancer, microbiology, medicine and psychology. Despite such consistent growth trends for some journals, this is not a universal feature. See **Table S1** for prominent journals ranked according to their average SA diversity value $\langle f_D \rangle_{j,1970-2018}$.

Discussion

With each new discovery – some large, others incremental – there is also a need to find its place in the order of things – some adding new layers to our understanding, and others filling in gaps. Classification systems are designed to manage the increasing volume of knowledge, so that it can be readily recorded, searched, explored and exploited in the pursuit to create new knowledge. From the Decimal Classification system (developed by expert committees and used in libraries around the world) to the Wikipedia category structure (a crowdsourced representation of our collective knowledge [62–64]), we are surrounded by ontologies that attempt to organize our common understanding. Likewise, the MeSH system aims to organize biomedical knowledge into a networked hierarchy that relates objects, methods, theory and other contextual metadata; notably, the traditional PACS system has recently been revamped into PhySH by adopting a similar concept-based hierarchy that is better suited for integrating the multiple sub-disciplines and facets that define the domain of physics [65].

We exploited the MeSH ontology structure to develop a dynamic and high-resolution map of cross-domain integration, which contributes to prior efforts to visualize the biomedical knowledge network [8, 18, 33]. In particular, we developed methods to visualize MeSH co-occurrence and quantify cross-domain diversity. Macro-level analysis of MeSH co-occurrence networks identifies three robust knowledge clusters: the vast universe of microscopic biological entities and structures; systems, disease and diagnostics; and biological and social phenomena capturing emergent properties, processes and functions. Research at the health, behavioral and brain science frontiers typically integrate these knowledge domains, signaling the emergence and future potential of convergence science [20, 21, 25, 29, 56, 66, 67]. The convergence nexus of Health Care (N), Behavior and Behavior Mechanisms (F01) and Information Science (L01) is a prime example, making way for transdisciplinary brain science [29] to map and model brain circuits [68] that are fundamental to addressing the grand challenge regarding the “global burden of mental disorders” [69, 70]. We reinforced these macro trends by micro-level analysis of article-level MeSH diversity, which increased by 40% over the entire study period from 1970 to 2018 – see **Fig. 4(B)**. This shift can be partly explained by a reduction in the prevalence of mono-domain research, analog to the simultaneous reduction of solo-authored research [30].

Comprehensive analysis of the knowledge network can also identify periods of disruption. By assessing the dynamics of MeSH usage across the entire PubMed index, we identified periods in which MeSH increasingly fluctuate between knowledge clusters (see **Fig. S6**). To identify the particular MeSH that bridge different knowledge communities we developed a cross-cluster bridge metric in Eq. (1). **Figure 3** shows the emergence of technology (J01) and informatics (L01) as prominent convergence bridges, reflecting the highly generalizable, scalable and codifiable characteristic of techno-informatic tools and algorithms that accelerate scientific discovery by facilitating high-throughput, measurement, data integration and analysis. **Figure 4(A)** further indicates the prevalence of this potent combination, which rapidly emerged in the early 1990s during the genomics revolution. Notably, this endeavor highlights the role of cross-disciplinary collaboration between scholars from traditional biology and computer science departments, which provided an early example of successful convergence, likely owing to the consortium science model whereby teams of teams organize with a common goal to share benefits equitably within and beyond institutional boundaries [28]. In related work, we show that research integrating subject areas that span relatively larger disciplinary distances is more impactful when executed by cross-disciplinary teams as opposed to mono-disciplinary teams [29]. We provide complementary support, showing that medium and large-scale teams have a notable advantage integrating multiple research domains – see **Fig. 4(C)**. Viewed from a different bureaucratic perspective, we observe variable levels and growth rates of convergence in journals, possibly owing to the multi-disciplinary composition (or lack thereof) of journal editorial boards.

In summary, techno-informatic capabilities are increasingly essential to the biomedical frontier. As illustrated by **Fig. 4(A)**, these distinct inputs are increasingly found as complements rather than substitutes – for the period 2000-2018 we estimate that $\langle f_x \rangle \approx 8.2\%$ of research articles relied on techno-informatic capabilities in tandem (J+L); this frequency corresponds to a 291% growth over the J+L convergence levels in 1980. If the future relies on harnessing the combined power of human and machine intelligence, then the development of *human-in-the-loop* and Man-Machine Systems (J01.897.441) “in which the functions of the man and the machine are interrelated and necessary for the operation of the system” will require transdisciplinary domains such as bio-mechatronics to flourish by harnessing convergence [71]. For this reason, scientists are increasingly in need of knowledge maps to navigate the realm of possibilities and to thereby which conceptual bridges to cross and which to avoid.

Methods

Subject Area (SA) classification using MeSH. We used the 2020 MeSH classification tree, which includes 29,638 descriptors that are organized in a tree-like structure denoting their hierarchical relations. MeSH descriptors are assigned to biomedical publications through an indexing process performed by examiners at the US National Library of Medicine (NLM). With on average 12 MeSH per article, this ontology facilitates topic mapping and topic co-occurrence analysis at multiple levels of specificity [18]. We restrict our analysis to the “Major Topic Headings” for each article, which are indicated in each PubMed article page by an asterisk * next to the MeSH term; these Major MeSH account for roughly 1 in 3 MeSH descriptors, and so with on average 4 Major MeSH these annotations are sufficient to identify the article’s core content. As such, we use these publication-level MeSH to determine the topical Subject Areas (SAs), as indicated by the 10 pre-defined science-oriented MeSH branches (A, B, C, D, E, F, G, J, L, N).

Major MeSH Descriptors: refinement to 1st and 2nd branch level representation. For each publication p , we extracted the set of Major MeSH terms (as indicated by an asterisk in PubMed records) and represent them by the vector \vec{m}_p containing 29,638 elements, each representing a distinct MeSH term. We then map each MeSH term to its corresponding tree location, which specifies its classification among the 10 science-oriented MeSH branches. To be specific, we define a generic operator O_M which takes the vector \vec{m}_p and maps these counts to a combined count vector $\vec{S}A_p^{(2)}$ with 104 elements representing all L_2 MeSH: $O_M^{(2)}(\vec{m}_p) = \vec{S}A_p^{(2)}$. Similarly, we define the operator $O_M^{(1)}(\vec{S}A_p^{(2)}) = \vec{S}A_p^{(1)}$, which maps the L_2 MeSH counts to their L_1 branches.

In order to count co-occurrences, we take each $\vec{S}A$ and denote the binary SA vector $B_p = \text{Sign}(\vec{S}A)$, which reduces each element value to either 0 or 1. For an article with M_p non-zero elements, we then count all $\binom{M_p}{2}$ pairwise permutations which we record in a normalized co-occurrence matrix, given by $\mathbf{M}_p^{(1)}$ ($\mathbf{M}_p^{(2)}$) for the L_1 (L_2) representation. Each matrix is normalized to unity such that the total of all subelements $\sum_{i,j} \mathbf{M}_{p,ij} = 1$. This normalization step ensures that each publication contributes an equal share to the annual co-occurrence matrix, given by $\mathbf{M}_y^{(1)} = \sum_{p \in y} \mathbf{M}_p^{(1)} = N(y)$, where $N(y)$ is the total number of articles analyzed from year y (with similar definition for the L_2 level).

Calculation of the cross-cluster bridge score. Motivated by the bridge centrality index [53], we define the knowledge bridge score β_i of node i , given by

$$\beta_i = \sum_{C_I, C_J \in C \text{ and } C_I \neq C_J} D_{IJ} W_{iJ}, \quad (1)$$

which first requires identifying nodes belonging to distinct clusters, calculated here using the Louvain algorithm [34]. Here C represents the set of connected clusters in the giant component of an undirected network, and C_J represents a cluster that is different from the cluster C_I containing a given node i . We define D_{IJ} to be the distance between cluster C_I and C_J , measured as the inverse of the sum of weights of edges between the clusters, represented as $D_{IJ} = W_{IJ}^{-1} = (\sum_{i \in C_I \text{ and } j \in C_J} W_{ij})^{-1}$. Similarly, W_{iJ} is the sum of weights of edges between node i and all other nodes belonging to cluster C_J . For our purposes, we define the link weights as empirical co-occurrence values, $W \equiv \mathbf{M}_i^{(2)}$. Hence, individual MeSH terms (nodes) that play key roles in bridging knowledge clusters have high β_i values; contrariwise, nodes that are only connected to nodes belonging to their own cluster have $\beta = 0$.

Since $M_t^{(2)}$ tallies are proportional to the total number $N(t)$ of articles published in year t , which are generally increasing, we instead focus on the rank associated with each β_i score, denoted by $r_{\beta,i}$. **Figure S3** shows the rank dynamics of the MeSH in each cluster exhibiting significant growth or decline over the study period. To address how to compare ranks of nodes from clusters of varying size (measured as the total number of nodes within the cluster I , denoted by $|C_I|$), then we define the normalized Bridge rank score as $R_i = r_{\beta,i}/|C_I|$, as plotted in **Figure 3**.

Based upon each time series $R_{i,t}$ calculated at the 1-year time resolution, we identified emerging bridges using the following criteria: (i) The node is on average ranked in the top-20 of its own cluster; (ii) the time series is at least half as long as the entire observation period from 1970 to 2018; (iii) There is a significant positive or negative trend, as determined by linear regression, such that the trend coefficient P-value is smaller than 0.01; (iv) the trend coefficient magnitude is sufficiently large, in magnitude > 0.1 . These criteria identify 8 emerging knowledge bridges: E05, F01, F02, G07, J01, L01, N04 and N05.

Data Availability: All data analyzed here are openly available from PubMed API, the MeSH tree prescribed by the NLM (see <https://meshb.nlm.nih.gov/treeView>) and the 2018 Web of Science JCR list of Impact Factors.

Acknowledgments

IP acknowledges funding from the Eckhard- Pfeiffer Distinguished Professorship Fund; IP and AMP acknowledge support from NSF grant 1738163 entitled ‘From Genomics to Brain Science’. AMP acknowledges financial support from a Hellman Fellow award that was critical to completing this project. Any opinions, findings, and conclusions or recommendations expressed in this paper are those of the authors and do not necessarily reflect the views of the funding agencies.

Author Contributions

DY analyzed and visualized the data; IP performed research and participated in the writing of the manuscript; AMP performed the research, drafted the manuscript, collected, analyzed, and visualized the data.

Additional Information

Supplementary Information accompanies this paper.

Competing financial interests The authors declare no competing financial interests.

-
- [1] Fleming, L. Recombinant uncertainty in technological search. *Management Science* **47**, 117–132 (2001).
 - [2] Börner, K. *Atlas of science: Visualizing what we know* (MIT Press, 2010).
 - [3] Börner, K. *Atlas of knowledge: Anyone can map* (MIT Press, 2015).
 - [4] Börner, K. *Atlas of Forecasts: Modeling and Mapping Desirable Futures* (MIT Press, 2021).
 - [5] Börner, K., Chen, C. & Boyack, K. W. Visualizing knowledge domains. *Annual review of information science and technology* **37**, 179–255 (2003).
 - [6] Fleming, L. & Sorenson, O. Science as a map in technological search. *Strategic management journal* **25**, 909–928 (2004).
 - [7] Börner, K. *et al.* Design and update of a classification system: The UCSD map of science. *PloS one* **7**, e39464 (2012).
 - [8] Shi, F., Foster, J. G. & Evans, J. A. Weaving the fabric of science: Dynamic network models of science’s unfolding structure. *Social Networks* **43**, 73–85 (2015).
 - [9] Saket, B., Scheidegger, C., Kobourov, S. G. & Börner, K. Map-based visualizations increase recall accuracy of data. In *Computer Graphics Forum*, vol. 34, 441–450 (Wiley Online Library, 2015).
 - [10] Pan, R. K., Petersen, A. M., Pammolli, F. & Fortunato, S. The memory of science: Inflation, myopia, and the knowledge network. *Journal of Informetrics* **12**, 656–678 (2018).
 - [11] Petersen, A. M., Pan, R. K., Pammolli, F. & Fortunato, S. Methods to account for citation inflation in research evaluation. *Research Policy* **48**, 1855–1865 (2018).
 - [12] Rzhetsky, A., Foster, J. G., Foster, I. T. & Evans, J. A. Choosing experiments to accelerate collective discovery. *Proceedings of the National Academy of Sciences* **112**, 14569–14574 (2015).
 - [13] Helbing, D. Accelerating scientific discovery by formulating grand scientific challenges. *The European Physical Journal Special Topics* **214**, 41–48 (2012).
 - [14] Kuhn, T. S. The essential tension: Tradition and innovation in scientific research. In *The third University of Utah research conference on the identification of scientific talent*, 162–174 (University of Utah Press Salt Lake City, 1959).
 - [15] March, J. G. Exploration and exploitation in organizational learning. *Organization science* **2**, 71–87 (1991).
 - [16] Leydesdorff, L. & Etkowitz, H. Emergence of a triple helix of university—industry—government relations. *Science and public policy* **23**, 279–286 (1996).
 - [17] Etkowitz, H. & Leydesdorff, L. The dynamics of innovation: from national systems and “mode 2” to a triple helix of university—industry—government relations. *Research policy* **29**, 109–123 (2000).
 - [18] Petersen, A. M., Rotolo, D. & Leydesdorff, L. A Triple Helix Model of Medical Innovation: Supply, Demand, and Technological Capabilities in terms of Medical Subject Headings. *Research Policy* **45**, 666–681 (2016).
 - [19] NSF. Nsf convergence accelerator. <https://www.nsf.gov/od/oia/convergence-accelerator/> (Accessed 2/2021).
 - [20] National Research Council. *Convergence: Facilitating transdisciplinary integration of life sciences, physical sciences, engineering, and beyond* (National Academies Press, Washington, D.C., 2014).

- [21] Eyre, H. A. *et al.* Convergence science arrives: how does it relate to psychiatry? *Academic Psychiatry* **41**, 91–99 (2017).
- [22] Colón, W. *et al.* Chemical biology at the us national science foundation. *Nature chemical biology* **4**, 511–514 (2008).
- [23] Pan, R. K., Sinha, S., Kaski, K. & Saramäki, J. The evolution of interdisciplinarity in physics research. *Scientific reports* **2**, 1–8 (2012).
- [24] Leahey, E. & Moody, J. Sociological innovation through subfield integration. *Social Currents* **1**, 228–256 (2014).
- [25] Sharp, P. A. & Langer, R. Promoting convergence in biomedical science. *Science* **333**, 527–527 (2011).
- [26] Helbing, D. Globally networked risks and how to respond. *Nature* **497**, 51–59 (2013).
- [27] Fleming, L. Perfecting cross-pollination. *Harvard Business Review* **82**, 22–24 (2004).
- [28] Petersen, A. M., Majeti, D., Kwon, K., Ahmed, M. E. & Pavlidis, I. Cross-disciplinary evolution of the genomics revolution. *Science advances* **4**, eaat4211 (2018).
- [29] Petersen, A. M., Ahmed, M. E. & Pavlidis, I. Grand challenges and emergent modes of convergence science. *e-print: SSRN 3755704* 1–46 (2020).
- [30] Wuchty, S., Jones, B. F. & Uzzi, B. The increasing dominance of teams in production of knowledge. *Science* **316**, 1036–1039 (2007).
- [31] Engeström, Y. & Sannino, A. Studies of expansive learning: Foundations, findings and future challenges. *Educational Research Review* **5**, 1–24 (2010).
- [32] MeSH. The mesh (medical subject headings) system: A controlled vocabulary thesaurus used for indexing pubmed articles. <http://www.ncbi.nlm.nih.gov/mesh> (Accessed 3/2020).
- [33] Leydesdorff, L., Rotolo, D. & Rafols, I. Bibliometric perspectives on medical innovation using the medical subject headings of pub med. *Journal of the American Society for Information Science and Technology* **63**, 2239–2253 (2012).
- [34] Blondel, V. D., Guillaume, J.-L., Lambiotte, R. & Lefebvre, E. Fast unfolding of communities in large networks. *Journal of Statistical Mechanics: Theory and Experiment* **2008**, P10008 (2008).
- [35] Wagner, C. S. *et al.* Approaches to understanding and measuring interdisciplinary scientific research (idr): A review of the literature. *Journal of informetrics* **5**, 14–26 (2011).
- [36] Yegros-Yegros, A., Rafols, I. & D’este, P. Does interdisciplinary research lead to higher citation impact? the different effect of proximal and distal interdisciplinarity. *PLoS one* **10**, e0135095 (2015).
- [37] Porter, A., Cohen, A., David Roessner, J. & Perreault, M. Measuring researcher interdisciplinarity. *Scientometrics* **72**, 117–147 (2007).
- [38] Porter, A. & Rafols, I. Is science becoming more interdisciplinary? measuring and mapping six research fields over time. *Scientometrics* **81**, 719–745 (2009).
- [39] Rotolo, D. & Messeni Petruzzelli, A. When does centrality matter? scientific productivity and the moderating role of research specialization and cross-community ties. *Journal of Organizational Behavior* **34**, 648–670 (2013).
- [40] Boyack, K. W. Mapping knowledge domains: Characterizing pnas. *Proceedings of the National Academy of Sciences* **101**, 5192–5199 (2004).
- [41] Petersen, A. M. Megajournal mismanagement: Manuscript decision bias and anomalous editor activity at plos one. *Journal of Informetrics* **13**, 100974 (2019).
- [42] Fleming, L. Breakthroughs and the “long tail” of innovation. *MIT Sloan Management Review* **49**, 69 (2007).
- [43] Youn, H., Strumsky, D., Bettencourt, L. M. & Lobo, J. Invention as a combinatorial process: evidence from us patents. *Journal of the Royal Society interface* **12**, 20150272 (2015).
- [44] Verhoeven, D., Bakker, J. & Veugelers, R. Measuring technological novelty with patent-based indicators. *Research Policy* **45**, 707–723 (2016).
- [45] Boyack, K. W. *et al.* Clustering more than two million biomedical publications: Comparing the accuracies of nine text-based similarity approaches. *PLoS one* **6**, e18029 (2011).
- [46] Foster, J. G., Rzhetsky, A. & Evans, J. A. Tradition and innovation in scientists’ research strategies. *American Sociological Review* **80**, 875–908 (2015).
- [47] Mane, K. K. & Börner, K. Mapping topics and topic bursts in pnas. *Proceedings of the National Academy of Sciences* **101**, 5287–5290 (2004).
- [48] Doudna, J. A. & Charpentier, E. The new frontier of genome engineering with CRISPR-Cas9. *Science* **346** (2014).
- [49] Takahashi, K. *et al.* Induction of pluripotent stem cells from adult human fibroblasts by defined factors. *cell* **131**, 861–872 (2007).
- [50] Benner, S. A. & Sismour, A. M. Synthetic biology. *Nature Reviews Genetics* **6**, 533–543 (2005).
- [51] Church, G. M. & Regis, E. *Regenesis: how synthetic biology will reinvent nature and ourselves* (Basic Books, 2014).
- [52] Hoshika, S. *et al.* Hachimoji DNA and RNA: A genetic system with eight building blocks. *Science* **363**, 884–887 (2019).
- [53] Jensen, P. *et al.* Detecting global bridges in networks. *Journal of Complex Networks* **4**, 319–329 (2016).
- [54] Markram, H. The Human Brain Project. *Scientific American* **306**, 50–55 (2012).
- [55] Grillner, S. *et al.* Worldwide initiatives to advance brain research. *Nature neuroscience* **19**, 1118–1122 (2016).
- [56] Roco, M., Bainbridge, W., Tonn, B. & Whitesides, G. *Converging Knowledge, Technology, and Society: Beyond Convergence of Nano-Bio-Info-Cognitive Technologies* (Springer, New York, 2013).
- [57] Lazer, D. *et al.* Life in the network: the coming age of computational social science. *Science* **323**, 721–723 (2009).
- [58] Fortunato, S. *et al.* Science of Science. *Science* **359**, eaao0185 (2018).
- [59] Harrison, D. A. & Klein, K. J. What’s the difference? diversity constructs as separation, variety, or disparity in organizations. *Academy of management review* **32**, 1199–1228 (2007).
- [60] Heller, A. *Renaissance man* (Routledge, 2015).
- [61] Simonton, D. K. After Einstein: Scientific genius is extinct. *Nature* **493**, 602–602 (2013).
- [62] Suchecki, K., Salah, A. A. A., Gao, C. & Scharnhorst, A. Evolution of wikipedia’s category structure. *Advances in complex systems* **15**, 1250068 (2012).
- [63] Akdag Salah, A., Gao, C., Suchecki, K. & Scharnhorst, A. The need to categorize: a comparative look at categorization in wikipedia and the universal decimal classification system. *Leonardo* **45**, 84–85 (2012).

- [64] Salah, A. A. A., Gao, C., Scharnhorst, A. & Suchecki, K. Design vs. emergence: Visualisation of knowledge orders. *Places & Spaces: Mapping Science: 7th Iteration (2011): Science Maps as Visual Interfaces to Digital Libraries* (2011).
- [65] Smith, A. From PACS to PhySH. *Nature Reviews Physics* **1**, 8–11 (2019).
- [66] National Research Council. *Facilitating interdisciplinary research* (National Academies Press, Washington, D.C., 2005).
- [67] Linkov, I., Wood, M. & Bates, M. Scientific convergence: Dealing with the elephant in the room. *Environmental Science and Technology* **48**, 10539–10540 (2014).
- [68] Jorgenson, L. A. *et al.* The brain initiative: developing technology to catalyse neuroscience discovery. *Philosophical Transactions of the Royal Society B: Biological Sciences* **370**, 20140164 (2015).
- [69] Kessler, R. C. *et al.* The global burden of mental disorders: An update from the WHO World Mental Health (WMH) surveys. *Epidemiology and Psychiatric Sciences* **18**, 23–33 (2009).
- [70] Dzau, V. J. & Balatbat, C. A. Reimagining population health as convergence science. *The Lancet* **392**, 367–368 (2018).
- [71] Li, Z., Yang, C. & Burdet, E. Guest editorial an overview of biomedical robotics and bio-mechatronics systems and applications. *IEEE Transactions on systems, man, and cybernetics: Systems* **46**, 869–874 (2016).

Supplementary Information – Appendix Text, Figure S1-S6 & Table S1

Biomedical Convergence Facilitated by the Emergence of Technological and Informatic Capabilities

Dong Yang¹, Ioannis Pavlidis², Alexander M. Petersen¹

¹Department of Management of Complex Systems, Ernest and Julio Gallo Management Program, School of Engineering, University of California, Merced, California 95343, USA;

²Computational Physiology Laboratory, University of Houston, Houston, Texas 77204, USA

Appendix Text

S1. MeSH cluster dynamics indicate periods of knowledge network reorganization.

The knowledge network dynamics, in particular bursts of cluster size variation exhibited in **Figure 2(D)**, allude to paradigm shifts mediated by scientific discovery. To identify particularly disruptive periods in the knowledge network, we developed a network method for identifying fluctuations of individual MeSH constituents across clusters by tracking the entry and exit of constituents between sequential 1-year periods.

To systematically track relations between MeSH branches, at either the L_1 or L_2 level, this straightforward method requires a flexible system for labeling clusters. To this end we designed a cluster-tagging method that first relies on identifying the stable subclusters, or cliques. In the present case, these cliques correspond to MeSH that are always observed in the same cluster together – in particular within co-occurrence clusters calculated at the 1-year level.

Figure S6(A) shows the MeSH cliques for the L_1 and L_2 levels. For example, an interesting cross-SA clique observed at the L_2 level is the dyad formed by “Technology, Industry, and Agriculture” (J01) and “Biomedical and Dental Materials” (D25); another mono-SA clique is the one formed by seven L_2 branches (D01, D02, D03, D04, D09, D10, D27), all from the L_1 D-branch. Hence, these stationary cliques are motifs that uniquely identify an arbitrary cluster C_x according to its constituent cliques.

By way of example, **Fig. S6(B)** shows the cluster C_c which contains the D-clique described above in two subsequent years. Consequently, an arbitrary MeSH denoted by i belonging to C_c in year t and $t + 1$ is stationary with respect to the cliques. Alternatively, consider an arbitrary MeSH j which was a member of C_a (identified by two particular cliques) and C_e in the next year (identified by two cliques, one from C_a and one altogether new one). In this case, the MeSH j (indicated by orange) has partially switched clusters. Finally, consider an arbitrary MeSH k (indicated by red) which was a member of C_b (identified by a single clique) and C_d in the next year (identified by a completely different clique); this case corresponds to minimal continuity (maximal discontinuity) with respect to cluster member cliques.

To quantify aggregate cluster dynamics, we assign each MeSH (represented generically by the index m) a set of labels $Q_{m,t} = \{q_1, \dots, q_n\}$ corresponding to each of the n unique cliques present, as indicated by q , for a given year t . We then calculate the Jaccard distance $\Delta J_m = 1 - |Q_{m,t} \cap Q_{m,t+1}| / |Q_{m,t} \cup Q_{m,t+1}|$. Hence, $\Delta J_m = 0$ corresponds to maximal continuity (since $|Q_{m,t} \cap Q_{m,t+1}| = |Q_{m,t} \cup Q_{m,t+1}|$). Conversely, $\Delta J_m = 1$ corresponds to maximal discontinuity (since $|Q_{m,t} \cap Q_{m,t+1}| = 0$). When there is a partial shift in cluster member cliques, then we obtain intermediate values, $0 < \Delta J_m < 1$.

Figure S6(C) indicates the periods with the highest levels of MeSH network reorganization, characterized by $\Delta J_m > 0$ values (indicated by orange and red curves). These results are consistent for both the L_1 and L_2 resolution levels. MeSH data aggregated at the L_1 level indicates a period of heightened MeSH cluster dynamics starting in the roughly 2000 and continuing in bursts up to present. Additional inspection at the L_2 level indicates periodic fluctuations occurring over time, but again with heightened turbulence in the early 1980s, and in the years around 2010. We interpret these heightened periods of MeSH cluster discontinuity as indicators of individual MeSH that emerge as cross-cluster knowledge bridges that integrate distinct knowledge domains, a hallmark of biomedical convergence in topical SA space. As such, the objective of this method is to the objective of which is to identify and justify disruptive periods analyzed in detail in the following sections.

S2. Techno-informatic capabilities facilitate biomedical convergence around brain, behavior and health science.

Concurrent co-occurrence of MeSH pairs (denoted by j and j') that are close neighbors of a given MeSH (i.e., the ego node, i) is indicative of recombinant knowledge domains mediated by i . To analyze this triadic closure phenomena as it relates to cross-domain convergence, we explored dynamic patterns occurring in the subset of $M_{jj'}^{(2)}$ values among the most prominent co-occurring neighbors of a given MeSH. In particular, we focused on the co-occurrence dynamics for each of the convergence bridges identified in Fig. 3.

For each convergence bridge MeSH, we then selected the ten most frequently co-occurring MeSH for the denoted period. Figure S4 shows the subset of $M^{(2)}$ values visualized as a subnetwork. For a given period, the top ten co-occurring neighbors (j) are sorted in clockwise fashion starting from the top, with nodes sized proportional to $M_{ij}^{(2)}$. To facilitate visual inspection, each MeSH's SA is indicated by its node/label color. Links are plotted with thickness and shade proportional to $M_{jj'}^{(2)}$, thereby indicating the cross-domain linkages among prominent neighbors that are facilitated by i . Each node includes its MeSH identifier and a knowledge cluster identifier, the latter indicated by a gray scale gradient.

The most significant feature of each convergence bridge are as follows: "Investigative Techniques" (E05) integrate all clusters with high SA diversity. "Behavior and Behavior Mechanisms" (F01) integrates health, "Physiological Phenomena", "Eukaryotes" and "Pathological Conditions, Signs and Symptoms" domains. F01 and "Psychological Phenomena" (F02) increasingly incorporate "Information Science" (L01) and "Investigative Techniques". "Physiological Phenomena" (G07), which exhibits a high co-occurrence with "Food and Beverages" research, representing the increasingly lucrative domain of human health science, also exhibits high diversity of cross-SA and cross-cluster. "Technology, Industry, and Agriculture" (J01) increasingly integrates from the 1990s onward with the "Chemical and Drugs" domain, highlighting the role of academic-industry-government cross-industry triple-helix [16, 17] underlying the pharmaceutical industry. L01 integrates with "Mathematical Concepts" to facilitate research investigating "Behavior and Behavior Mechanisms" by leveraging technology providing non-invasive "Investigative Techniques". And both "Health Services Administration" (N04) and "Health Care Quality, Access, and Evaluation" (N05), which have become highly coupled mirrors of each other, have in the last decade incorporated "Information Science" methods for clinical diagnosis and classification of "Pathological Conditions, Signs and Symptoms" and overall health care program assessment.

S3. Outer-product method for measuring categorical diversity and disparity.

We leverage a generic tensor-product method that takes as input a weighted vector and yields a scalar diversity measure based upon categorical mixing. While the result of our approach is nearly identical to the Blau index (also referred to as the Gini-Simpson index), our diversity measure is motivated by way of dyadic co-occurrence rather than the standard formulation motivated around repeated sampling. Within the present context, the weighted vector of category counts is the SA decomposition of an article, given by $\vec{S}A_p^{(1)}$ or $\vec{S}A_p^{(2)}$. The resulting metric, represented by $f_{D,p}$, quantifies the degree of cross-domain co-occurrence and is a bounded statistic in the range $[0, 1)$.

Calculating $f_{D,p}$ begins with the outer-product $\vec{S}A_p \otimes \vec{S}A_p$, where \otimes is the outer tensor product. The resulting matrix represents dyadic combinations of categories as opposed to permutations (i.e., capturing the subtle difference between an undirected and directed network). While we did not explore it further, this matrix formulation may also give rise to higher-order measures of diversity associated with the eigenvalues of the outer-product matrix.

We normalize the resulting outer-product matrix so that our analysis is not systematically biased by increase in the number of MeSH per paper over time; see [18] for secular growth in the number of MeSH per article, reflecting growth of the MeSH ontology accompanied by growth in the length and breadth of published research. All steps together, the normalized co-occurrence matrix \mathbf{D}_p is given by

$$\mathbf{D}_p \equiv \frac{U(\vec{S}A_p \otimes \vec{S}A_p)}{\|U(\vec{S}A_p \otimes \vec{S}A_p)\|}. \quad (\text{S1})$$

Without loss of generality, this definition involves $U(\mathbf{G})$, an operator yielding the upper-diagonal elements of the arbitrary matrix \mathbf{G} (i.e., representing the undirected co-occurrence network among subcategories); $\|\dots\|$ indicates the matrix total calculated by summing across all matrix elements. The subtle difference between the Blau index arises from $U(\mathbf{G})$, which is imposed to capture the difference between combinations rather than permutations (or directed versus undirected network). Hence, this perspective offers a new pathway to this fundamental diversity measure by way of co-occurrence rather than repeated sampling.

Hence, $\mathbf{D}_p(\vec{S}A_p)$ tabulates the weighted product across all undirected SA-SA pairs. We then define the co-occurrence diversity as the scalar quantity given by

$$f_{D,p} = 1 - \text{Tr}(\mathbf{D}_p) \in [0, 1), \quad (\text{S2})$$

where Tr is the matrix trace, corresponding to the sum of diagonal elements in \mathbf{D}_p . Hence, $f_{D,p}$ is the tally of off-diagonal elements in \mathbf{D} . Articles featuring a single SA have value $f_{D,p} = 0$, whereas articles featuring multiple SA have values in the range $0 < f_{D,p} < 1$. Regarding the upper limit, when all vector elements have equal values then $f_{D,p} = (d-1)/(d+1)$, where d is the dimension of the categorical vector (for the Blau index the upper limit is instead $d-1/d$). In the present case $d = 10$ and so the maximum $f_{D,p}$ value is $9/11$. The average article diversity by publication year, denoted by $\langle f_D(t) \rangle$, is representative of a characteristic article since $f_{D,p} \in [0, 1)$ is bounded.

By way of example, consider a decomposition across only 6 SA, and the particular case of an article with 4 MeSH belonging to 3 different SA, e.g. $\vec{S}A_p = \{1, 2, 0, 0, 1, 0\}$. Calculation of the co-occurrence matrix $\mathbf{D}_p(\vec{S}A_p)$ in Eq. (S1) yields

$$\mathbf{D}_p(\vec{S}A_p) = \begin{pmatrix} \frac{1}{11} & \frac{2}{11} & 0 & 0 & \frac{1}{11} & 0 \\ 0 & \frac{4}{11} & 0 & 0 & \frac{2}{11} & 0 \\ 0 & 0 & 0 & 0 & 0 & 0 \\ 0 & 0 & 0 & 0 & 0 & 0 \\ 0 & 0 & 0 & 0 & \frac{1}{11} & 0 \\ 0 & 0 & 0 & 0 & 0 & 0 \end{pmatrix}$$

with $\|U(\vec{S}A_p \otimes \vec{S}A)\| = 11$. The categorical diversity is the total across the off-diagonal elements, $f_{D,p} = 5/11$.

For comparison, consider the representation of an article with the same number of metadata entities that all fall into just the second category, $\vec{S}A_p = \{0, 4, 0, 0, 0, 0\}$. In which case

$$\mathbf{D}_p(\vec{S}A_p) = \begin{pmatrix} 0 & 0 & 0 & 0 & 0 & 0 \\ 0 & 1 & 0 & 0 & 0 & 0 \\ 0 & 0 & 0 & 0 & 0 & 0 \\ 0 & 0 & 0 & 0 & 0 & 0 \\ 0 & 0 & 0 & 0 & 0 & 0 \\ 0 & 0 & 0 & 0 & 0 & 0 \end{pmatrix}$$

and so $f_{D,p} = 1 - 1 = 0$.

What does this measure measure? Notably, $f_{D,p}$ accounts for both categorical differences (Shannon-like) and concentration disparity (Gini-like) [59]. On the first hand, articles with more variation in SA categories will correspond to larger $f_{D,p}$ values, as the number of non-zero off-diagonal elements is proportional to $\binom{M_p}{2} \sim M_p^2$, where M_p is the number of distinct SA present, which contributes to larger $f_{D,p}$; and on the second hand, the off-diagonal elements will be relatively larger in combination if the count values contained in $\vec{S}A_2$ are more evenly distributed, i.e., are not highly concentrated in just one category.

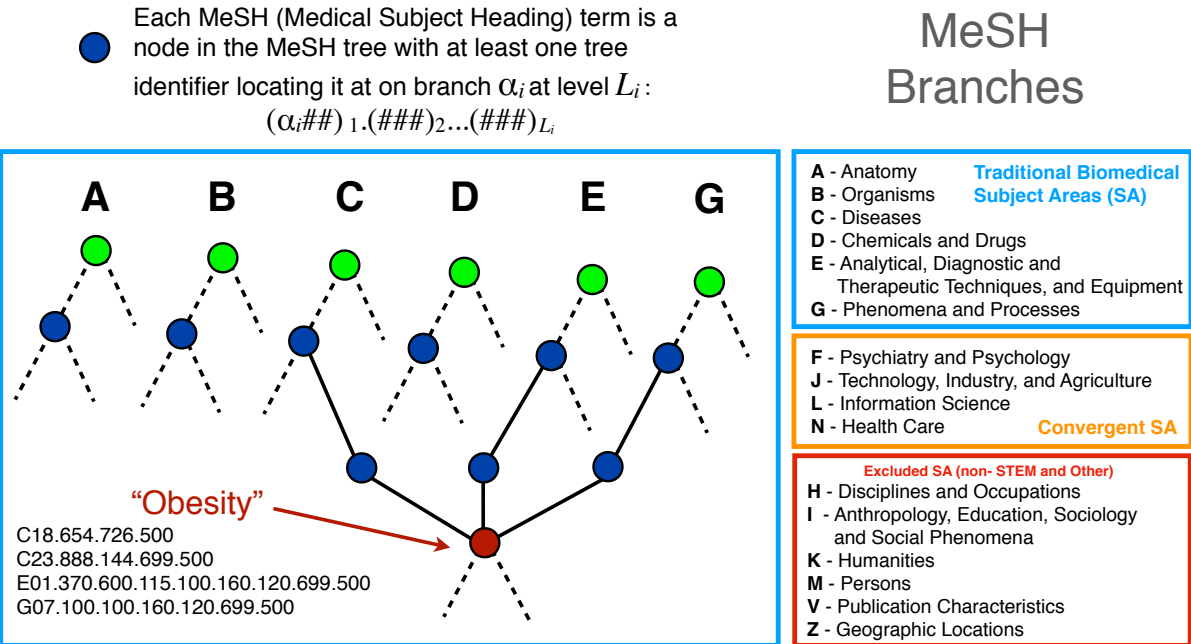


FIG. S1: **Schematic representation of the quasi-hierarchical MeSH tree.** We restrict this illustration to MeSH belonging to the core biomedical branches $\alpha = \{A, B, C, D, E, G\}$. The location of each MeSH m is given by the set of locations of the parent nodes directly above it. For example the MeSH “Overnutrition” with Tree Number C18.654.726 is located at the third level, and has daughter MeSH “Obesity” which has four Tree Numbers corresponding to three distinct branches (C, E and G): C18.654.726.500, C23.888.144.699.500, E01.370.600.115.100.160.120.699.500, G07.100.100.160.120.699.500. Hence, this particular MeSH maps onto three L_1 branches represented by $\vec{s}_A^{(1)} = \{0,0,2,0,1,0,1,0,0,0\}$.

TABLE S1: **Top-20 Convergent Journals.** Biomedical journals in the top-100 2018 JCR Impact Factor, ranked according to average categorical SA diversity over the period 1970 to 2018.

Journal (j)	Average SA diversity $\langle f_D \rangle_{j,1970-2018}$
Circ. Res.	0.556
J. Clin. Oncol.	0.549
J. Am. Coll. Cardiol.	0.511
Acta. Neuropathol.	0.509
Nat. Genet.	0.506
Gut	0.493
PNAS	0.483
Science	0.481
Ann. Intern. Med.	0.474
N. Engl. J. Med.	0.466
Cell	0.466
Nature	0.464
Eur. Heart J.	0.462
BMJ	0.459
Endocr. Rev.	0.456
Lancet	0.452
Clin. Microbiol. Rev.	0.436
Physiol. Rev.	0.434
Annu. Rev. Immunol.	0.400
CA. Cancer J. Clin.	0.389

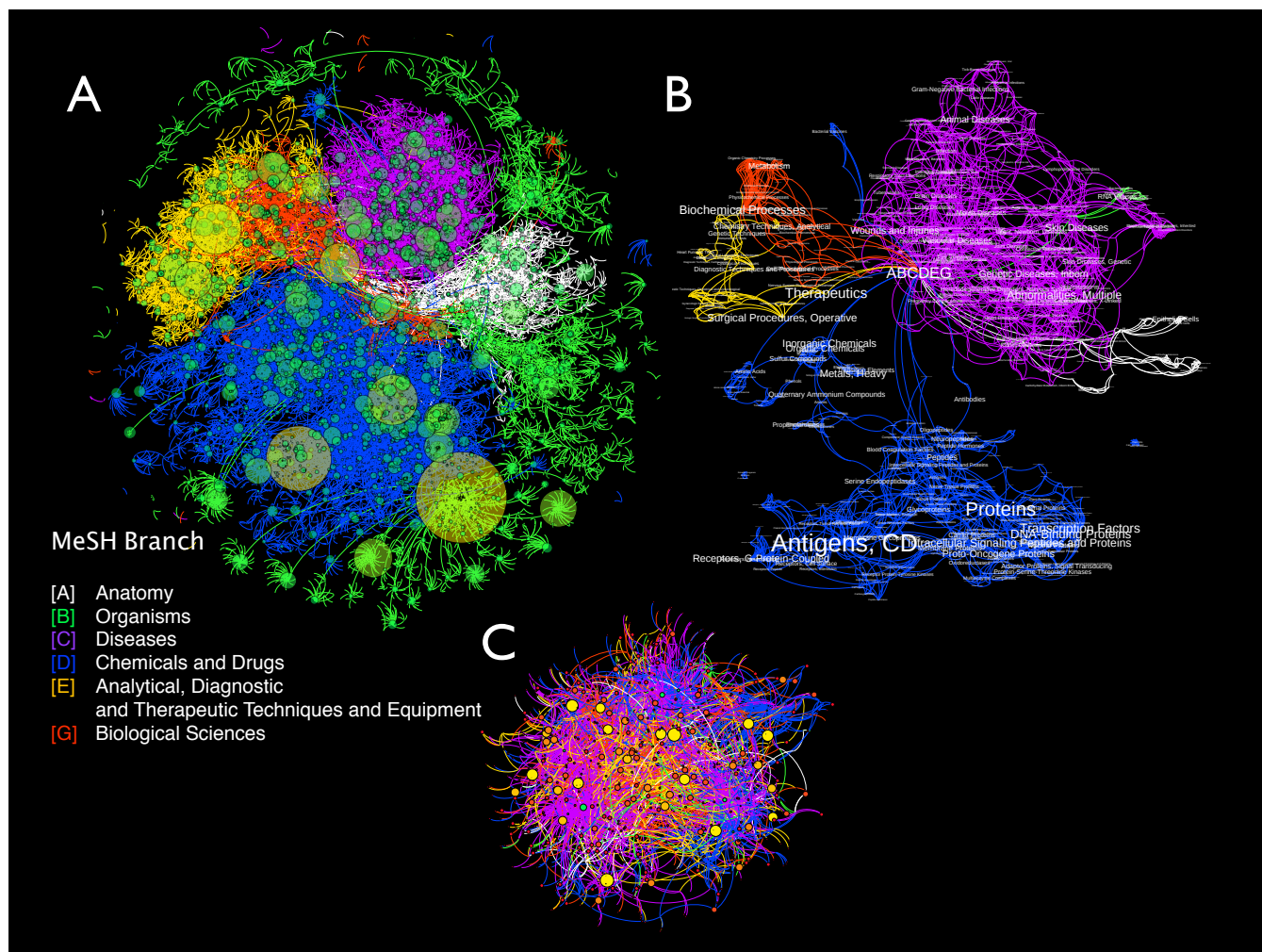


FIG. S2: **Structure and interconnectivity of the MeSH knowledge network.**(A) Network visualization of the MeSH branches $\alpha_i = \{A, B, C, D, E, G\}$. Size and color of nodes is proportional to the in-degree of the MeSH term (from higher tree levels). The color of the link is associated with the branch classification of the parent node. (B) MeSH network with most prominent nodes labeled for visual inspection. (C) The network of links that span different tree branches, $\alpha_i \leftrightarrow \alpha_j$.

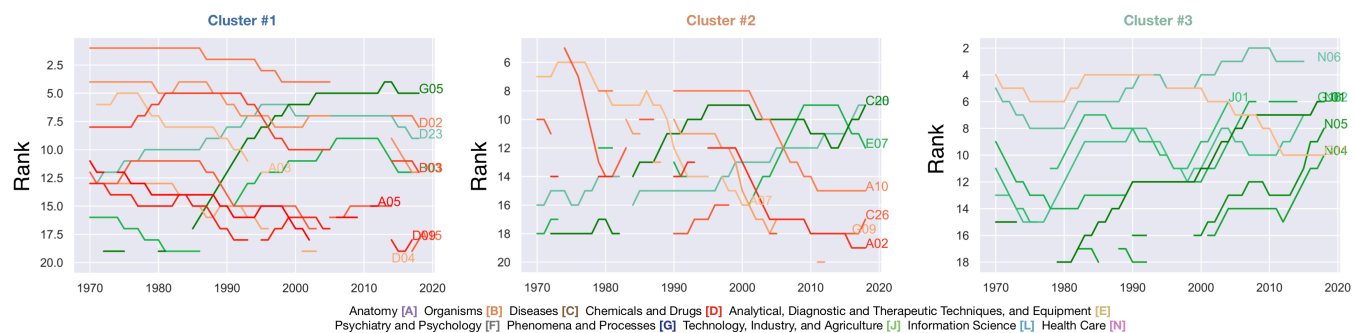


FIG. S3: **MeSH with high bridge rank and significant trends – by knowledge cluster.** Evolution of knowledge bridge ranks for individual MeSH that feature either sustained high bridge rank or significant positive (indicated by green) or negative (indicated by red) rank change over the entire period of analysis.

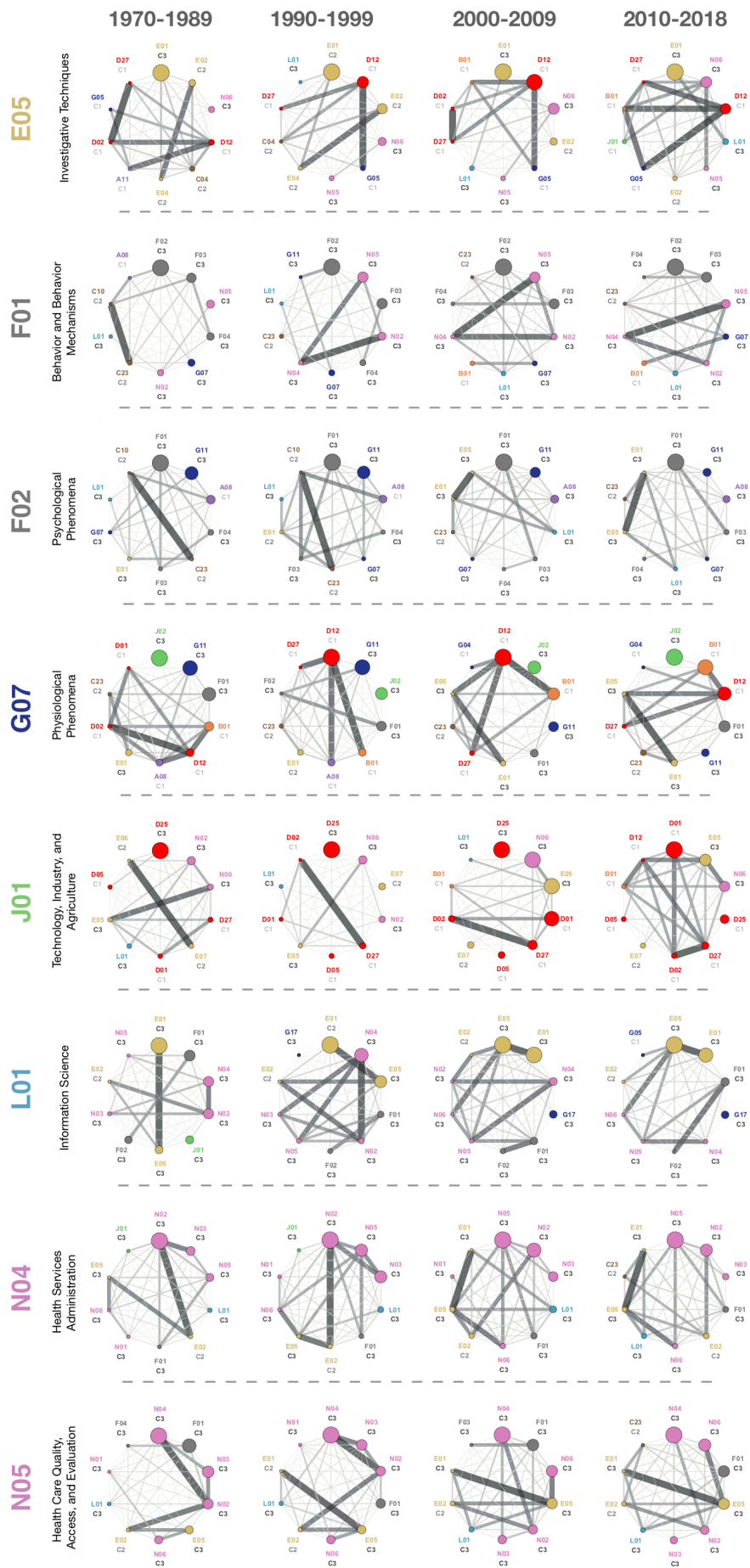


FIG. S4: Temporal network dynamics for 8 convergence bridges. Each row illustrates a MeSH term (i) identified as a convergence bridge. Each network is calculated using data from the indicated period, and shows the ten most frequently co-occurring MeSH – sorted clockwise, starting from the top, with nodes sized proportional to $M_{ij}^{(2)}$; each MeSH’s SA is indicated by its node/label color. Links are plotted with thickness and shade proportional to $M_{jj}^{(2)}$, thereby indicating the cross-domain linkages among prominent neighbors that are facilitated by i . Each node includes its MeSH identifier and a knowledge cluster identifier, the latter indicated by a gray scale gradient. For example, MeSH J01 “Technology, Industry, and Agriculture” (which is a member of C3 for the first three periods and subsequently transitioning to C1 in the most recent period) is highly connected to MeSH from all other clusters (C1-C3), in particular to L01 until its disassociation in the most recent period 2010-2018; interestingly, L01 “Information Science” diverged from J01 as early as the first period 1970-1989, subsequently becoming more strongly coupled with members of branch E and G.

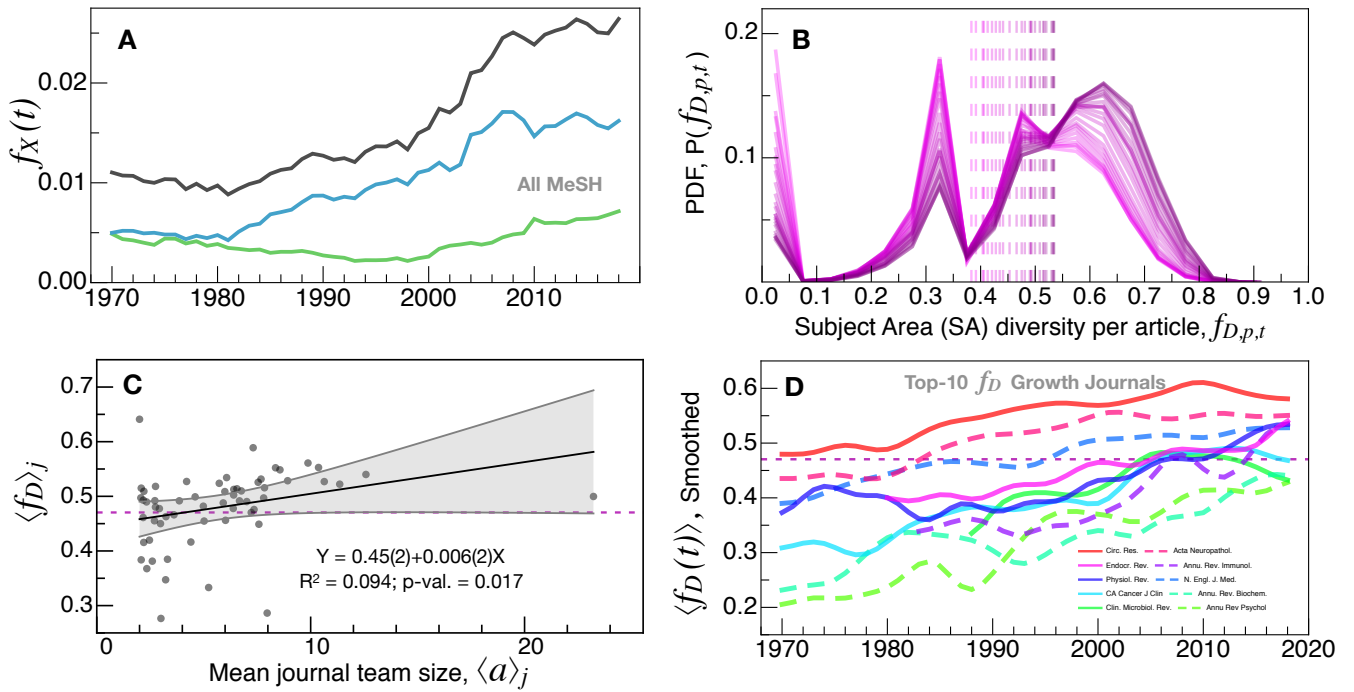


FIG. S5: **Cross-domain knowledge integration – supporting analysis.** (A) Analog to Fig. 4(A) but calculated using all MeSH (i.e., analyzing MeSH independent of Major/Minor status). (B) Probability distribution $P(f_{D,p})$ for each of the 3-year subsamples analyzed in Fig. 4(B). One notable shift is the decreased prevalence of mono-domain articles ($f_{D,p} = 0$) which is a large but not sole contributor to the increasing trend in average value, $\langle f_D(t) \rangle$ (shown as horizontal vertical dashed lines). Nevertheless, the right tail of the distribution is well defined and does not increase dramatically in range (i.e., the max diversity value is persistently around the value 0.9). The peak around value 1/3 (1/2) corresponds to articles with MeSH contributing equally to two (three) distinct SA and represents the first (second) mode of cross-domain convergence. (C) Robustness check for Fig. 4(C), showing positive relationship between average team size and cross-domain SA diversity calculated at the journal level (ANOVA p-val.= 0.017; shaded region is 99% CI). (D) Ten biomedical journals featuring the highest growth in average $f_{D,p}$ values over 1970-2018.

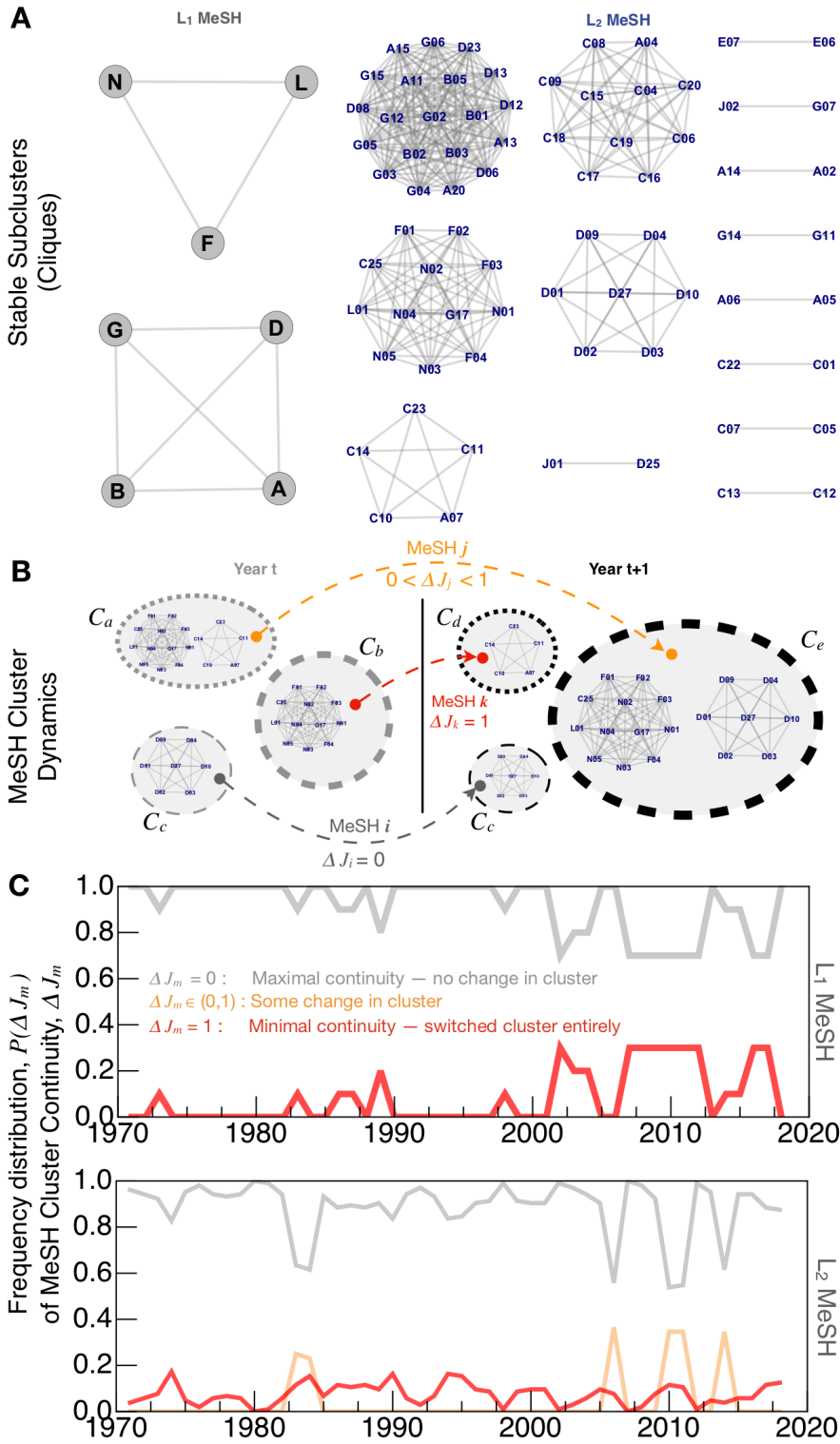


FIG. S6: Method for quantifying fluctuations of individual MeSH across knowledge clusters. Reorganization of co-occurrence networks are indicative of paradigmatic disruption and cross-domain bridge formation. Stable subclusters are groups of MeSH that always appear together in annual-level co-occurrence matrix Louvain clustering – see **Fig. 2(C)**. These cliques are used as an unique identification system for calculating the cluster continuity ΔJ_m of a given MeSH term m over sequential 1-year periods. (A) Cliques for the period 1970-2018 calculated for the L_1 (left) and L_2 (right) levels. (B) Schematic of the identification system for tracking cluster dynamics of individual m . For example, comparing MeSH i for the sequential year t and $t + 1$ periods, i stayed in the cluster C_c (identified as having the D-clique comprised of seven L_2 MeSH from the D-branch) and so there is maximal continuity of the cliques defining its surrounding cluster. Contrariwise, MeSH k transitioned from a cluster in t defined by a single clique that differs from the clique defining its cluster in $t + 1$; hence, this case corresponds to minimal continuity. The case of MeSH j is inbetween these extreme cases, whereby j transitions from a cluster in t that shares a common clique as the cluster in $t + 1$, but with differing second member clique. (C) Frequency distribution of continuity values ΔJ_m by year. Years with low MeSH cluster continuity feature higher frequencies of MeSH that switch knowledge clusters entirely (red) or partially (orange); conversely, periods with high cluster continuity, in which all m stay in the same cluster, corresponds to the gray curve approaching unity. The period with the highest levels of knowledge cluster discontinuity started in the early-2000s and peaked around 2010. Discontinuity peaks indicate the emergence of individual MeSH serving as cross-cluster bridges.